Evaluation of Spatial Variations in the Time and Frequency Dependence of Imaging Operators for Diffusion Tomography

H. L. Graber, J. Chang, and R. L. Barbour
State University of New York, Health Science Center at Brooklyn, Departments of Physiology and Biophysics and Pathology, 450 Clarkson Avenue, Brooklyn, New York 11203

J. Chang is also affiliated with Polytechnic University, Department of Electrical Engineering, 333 Jay Street, Brooklyn, New York 11201.

R. Aronson
Bioimaging Sciences Corporation, 64 Burnett Terrace, West Orange, New Jersey 07052

Abstract

Employing the framework of a perturbation model for optical diffusion tomography, the sensitivity and selectivity attainable from optical time- and frequency-domain, including phased array, measurements, are compared and contrasted. Monte Carlo simulations were used to calculate impulse-response functions in the interior of several homogeneous media. From the results, the impact on detected light due to small localized changes in absorption cross-section were computed. A feature unique to the frequency domain is the ability to qualitatively modify the depth profile of the weight amplitude by employing several sources in a phased array. In the case of single-source transmission measurements, a time-resolved measurement with a short integration time leads to enhanced ability to resolve deep-lying structures, by increasing the weight in deep regions relative to those near the surface. In contrast, as the source modulation frequency is increased in a frequency-domain measurement, the weight amplitude drops off most rapidly in regions farthest from the boundaries, and more slowly in more superficial regions. The significance of these findings for perturbation-based image recovery schemes is discussed.

Introduction

The use of time- or frequency-resolved illumination and detection schemes in optical studies of thick scattering media have been areas of intense research for several years. The number of reports on these topics, and the number of groups actively investigating them, have increased dramatically in that time [1-3]. The appeal of these schemes lies in their potential for enhancing the sensitivity and spatial discrimination of techniques designed to deduce the optical properties of the media, such as biological tissues, under investigation.

An underlying feature common to many of these studies is the goal of reducing the contribution to the detected signal made by many-times-scattered light. If this could be accomplished, it would be possible to analyze experimental results using existing algorithms developed in such fields as x-ray CT, diffraction tomography, and sonography. While the desirability of reducing the optical imaging problem to one that has already been solved is understandable, it is becoming increasingly clear that the maximum distance over which an unscattered or low-order scattered component exists to be detected is small [4], even if the ability to distinguish it from the background of highly scattered light were unlimited. It appears that solving the 3-D inverse scattering problem (ISP) is unavoidably necessary.

For this study, we started from the premise that the correct theoretical framework for image reconstruction is a perturbation approach to solving the 3-D ISP. The computations reported here were performed as one part of a project to assess the advantages and liabilities of image recovery based on time-domain and frequency-domain (either a single source or several in a phased array) data, and to compare all of these to the more easily implemented steady-state methods. The most useful information to gather for these purposes is the impulse-response functions at points in the interior of a medium, subsequent to

OSA Proceedings on Advances in Optical Imaging and Photon Migration, 1994, Vol. 21, R. R. Alfano (ed.)

illumination by an ideal pulse. All other quantities needed subsequently may be calculated from these.

Methods

Theoretical:

The perturbation model adopted for optical diffusion tomography [5] explicitly relates the differences between the light-intensity measurements at the surfaces of two media to differences between their internal structures. The mathematical forms of the *weight functions* relating them were derived from radiation transport calculations. For the case of time-resolved measurements, the weight at time t at a given point in the interior of a thick scattering medium, for specified source and detector locations, is proportional to the convolution of forward and adjoint light intensities at the point.

$$w_{ij}(t_1 - t_2) = \frac{S_j}{4\pi\Sigma_{t,i}^2 V_i}\int_{t_1}^{t_2}\int_0^t F_i^{s_j}(\tau)F_i^{d_j}(t-\tau)d\tau\,dt,$$

where $F_i^{s_j}$ and $F_i^{d_j}$ are the collision densities in voxel i due, respectively, to photons launched into the medium from the source and detector associated with the j^{th} measurement, S_j is the associated source strength, V_i is the volume of voxel i, and $\Sigma_{t,i}$ is the macroscopic total cross-section in voxel i. For the case of frequency-domain measurements, the weight at a given point and frequency ω is proportional to the ω-component of the time-resolved weight's Fourier transform. This, in turn, is equal to the simple product of Fourier transforms of the time-resolved forward and adjoint intensities [see reference 5 for derivations].

Numerical:

Time-resolved light intensities in the interior of thick scattering media were calculated by Monte Carlo simulations of photon propagation. In these, photons were treated as particles, and scatterings as classical collisions; the differential scattering cross-section was isotropic. The media modeled were a cylinder whose diameter was 20 mean free pathlengths (mfp; 1 mfp = $1/\Sigma_t$) and a slab 10 mfp thick. In the latter case, ten different sets of optical properties were chosen, matching each of five different degrees of homogeneous absorption (Σ_a/Σ_t = 0, .005, .01, .015, .02) with each of two ratios of internal to external refractive index (n = 1, 1.33). The cylinder was nonabsorbing with n = 1.33.

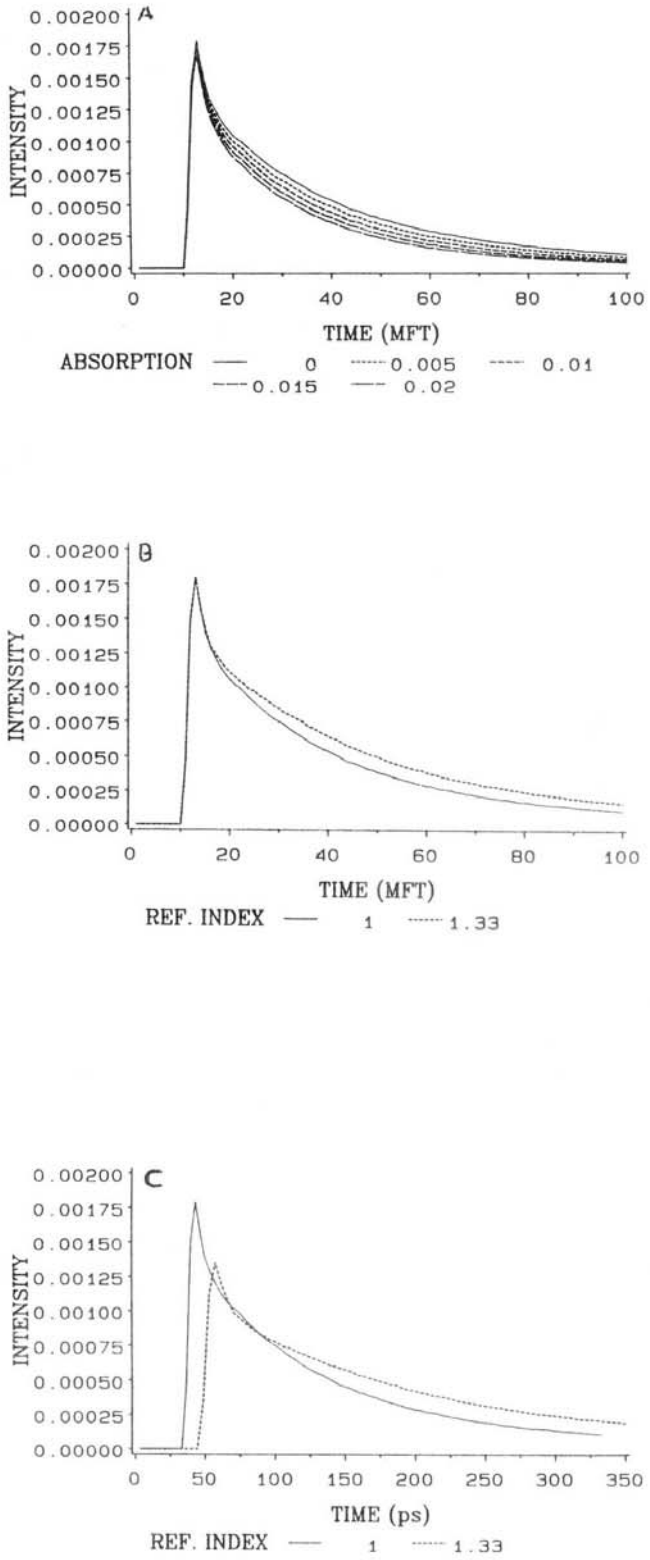

Figure 1 Examples of photon intensity *vs.* time in one interior voxel, following illumination by an ideal pulse at t = 0; mft = mean free times. Panel A: effect of increasing level of homogeneous absorption. Panel B: effect of increasing refractive index of medium. Panel C: preceding result rescaled to take account of change in speed of light.

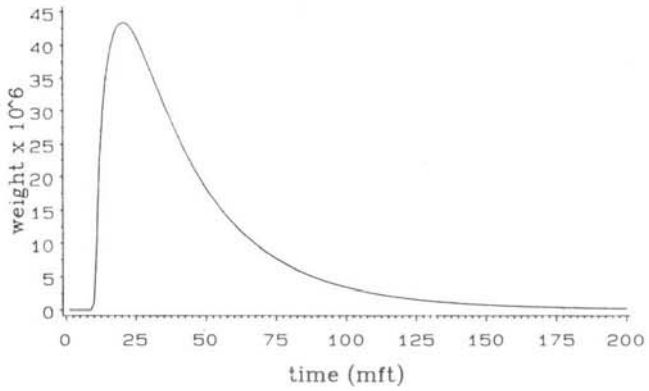

Figure 2 Example of a time-domain weight function in one voxel of a slab medium, 10 mean free paths (mfp) thick, and a transmission measurement.

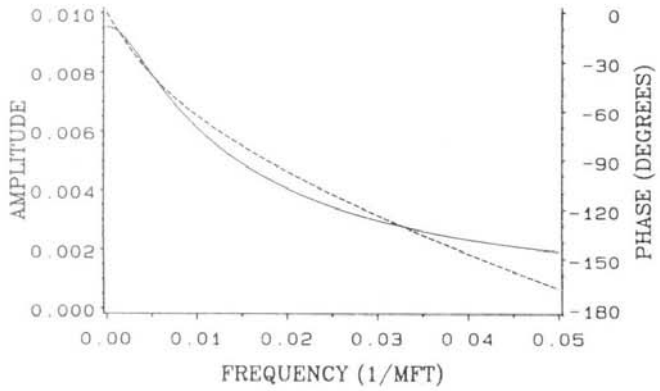

Figure 3 Example of a frequency-domain weight function in one voxel of a slab medium, 10 mfp thick, and a transmission measurement. Amplitude = solid curve; phase = dashed curve.

Results

Examples of time-resolved photon intensities in the interior of slab media are shown in Figure 1. For each curve, the intensity was calculated in a .75π–mfp^3 ring located 9–10 mfp below the illuminated surface and .5–1.0 mfp radially from the source line. In Panel A, the five curves correspond to media with five different absorption coefficients (Σ_a/Σ_t = 0, .005, .01, .015, .02). In Panel B, the two curves show the effect of changing the refractive index of the medium. These curves are replotted in Panel C, in which the different speeds of light, c, in the two media is also taken into account.

A time-resolved weight function for a voxel located at depth 5-6 mfp, and the case of n = 1.00, Σ_a = 0, is shown in Figure 2. This function was calculated for the case of a transmission measurement in which the source and detector are collinear. The amplitude (solid curve) and phase

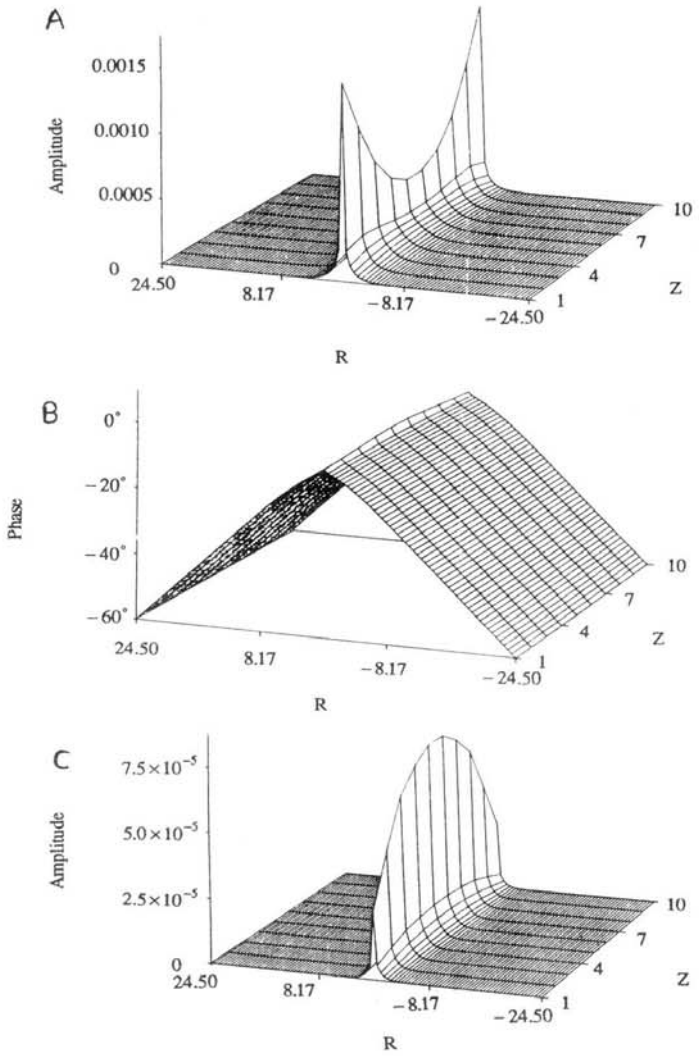

Figure 4 Freqency-domain weight functions, 10-mfp-thick slab medium, transmission measurement. Panel A: amplitude portion, 112.5 MHz modulation frequency (assuming 1 mfp = 1 cm). Panel B: phase portion, 112.5 MHz. Panel C: amplitude portion, 9 GHz .

(dashed curve) parts of the frequency-domain weight for the same volume and source and detector locations is shown in Figure 3. These weights are to be interpreted as the effect that a unit change in the Σ_a within the indicated volume would have on the flux across the surface at the site of the detector.

The data shown in Figure 4 are planar sections through frequency-domain weight functions for a single intensity-modulated source. The source and detector are collinear in a transmission measurement for the examples in this figure. Panels A and B contain, respectively, the amplitude and phase portions of the weight function for the slab with n = 1.33, Σ_a = 0, and a low modulation frequency, 112.5

MHz. Panel C shows the amplitude portion of the weight function when the modulation frequency is much higher, 9 GHz. The notable increase in weight amplitude with increasing distance from the surfaces seen in 4C is an interesting special case observed only when the medium is relatively thin and the source and detector axes intersect inside it, and is a consequence of the considerable component of first scatterings along these axes. This phenomenon is absent if the lines-of-sight of the source and detector do not intersect (data not shown) or if the medium thickness is increased (as in Fig. 6, below).

An example of an effect that can be achieved with phased arrays of sources is shown in Figure 5. Three sources were used, all at a modulation frequency of 150 MHz ($n = 1.00$, $\Sigma_a = 0$). The three source axes and the detector axis are coplanar; two sources are directed to the same surface as the detector, and straddle the detector, each being 5 mfp from it; the third source is directed to the opposite surface, collinear with the detector. Panels A and B show the amplitude and phase portions of the weight function when all three sources are in phase. Panels C and D are the corresponding weight function when the source in transmission is 180° out of phase with the other two. Other results, not shown, indicate it is possible to place the amplitude null at any desired point in the medium through judicious selection of the source locations and the amplitude and phase relations among them. We refer to this as the "source synthesis problem," and it may be viewed as analogous to antenna synthesis problems that arise in the field of synthetic aperture radar.

Figure 6 shows the spatial distributions of weight for three different illumination strategies, in one cross-sectional layer of the cylindrical medium. In each case the source and detector are collinear and the section illustrated contains the source and detector axes. The data were normalized by dividing the weight in each voxel by the sum of weights over the entire section. Panel 6A shows the normalized weight corresponding to a steady-state measurement. It can also be interpreted as the amplitude portion of the frequency-domain weight in the limit as the modulation frequency approaches 0, or as the time-domain weight in the limit as the detector integration time increases without bound. Panel B shows the normalized time-resolved weight for a measurement in which the detector time window was the first fifty mean free times (mft; 1 mft = $1/c\Sigma_t$) following the illumination pulse. Panel C shows the normalized frequency-domain weight for a measurement made at a modulation frequency of 5.625 GHz (assuming a mfp of 1.0 cm).

Sets of one-dimensional sections through surfaces such as those in Figure 6, along and across the source-detector line, are shown in Figure 7. The normalized weights are displayed on logarithmic scales so that results for several integration times or modulation frequencies can be displayed simultaneously. The effect of increasing integration time is shown in Panels A and B; the 500-mft result is essentially a steady-state weight function. It is evident from these that reducing integration time window to times slightly longer than the theoretical minimum transit time enhances sensitivity to regions at greater depth and resolution in the dimensions orthogonal to the source-detector line. The effect of increasing modulation frequency is shown in Panels C and D. These also show some enhancement of lateral resolution by employing higher frequencies, but along the source-detector line the weight amplitude falls more rapidly in the center of the section than it does near the surface. The absence of perfect bilateral symmetry in the curve in 7A and 7C is a simple consequence of the asymmetric geometric arrangement of voxels in the y-dimension.

Discussion

The perturbation approach to imaging of highly scattering media relates changes in detected light to changes in a medium's internal structure *via* weight functions such as those of which selected sections are shown in the Figures. This results in the conversion of the problem of reconstructing an image to one of solving a large system of linear equations. In practice, these systems are typically ill-conditioned [6]. We have elsewhere described numerical strategies for dealing with this problem, *e.g.*, the *regularized progressive expansion* [7] algorithm, but these are attempts to minimize its effects and do not eliminate it. The studies described above were undertaken, in part, as an attempt to deal with the *cause* of ill-conditioning, which is the rapid decrease in weight with increasing depth that is a feature of most measurement schemes.

The result shown for a phased-array frequency-domain measurement indicate one way in which the depth dependence of weight might be directly manipulable. The value of this approach would be limited, however, unless the ability to enhance the weight at points in the middle of the medium relative to that near the surfaces could be demonstrated. In addition, for this ability to be useful, it is necessary that computation of the correct amplitude and phase relations among the sources be a straightforward matter, and not in itself a difficult inverse problem. This source synthesis problem is presently being

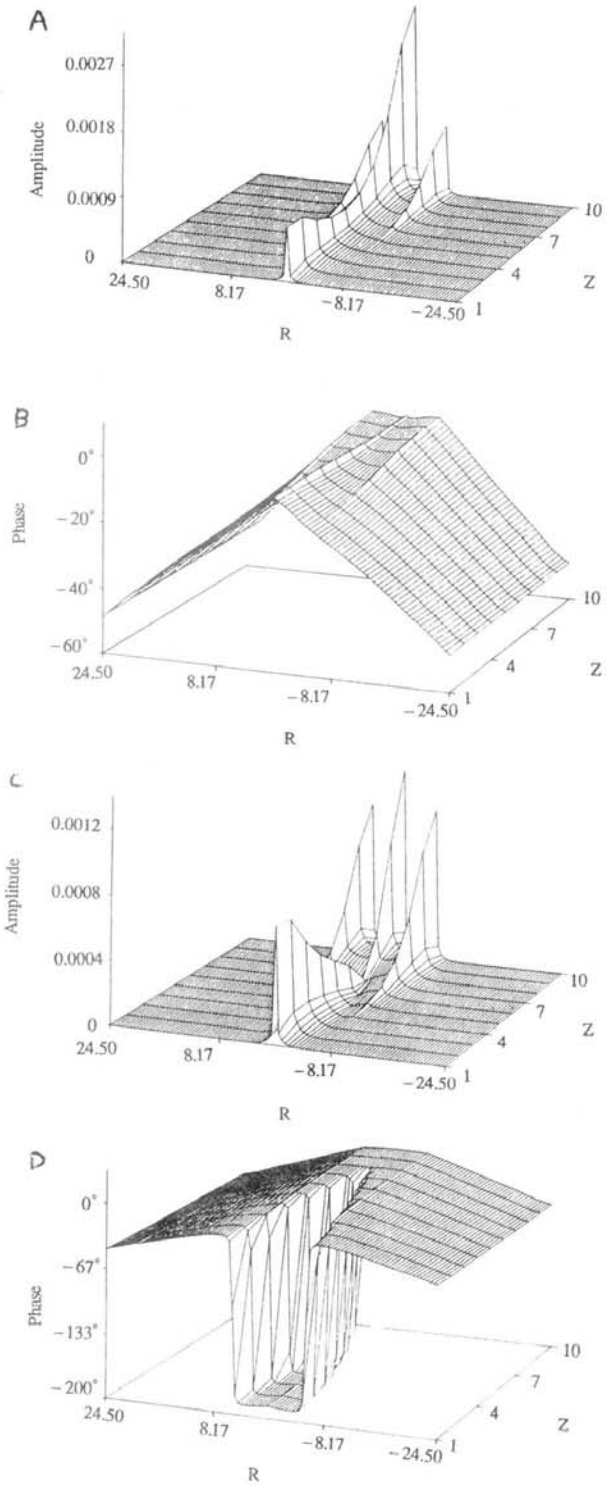

Figure 5 Phased-array weight functions; 10-mfp-thick slab medium; 3 sources, all with the same DC strength and AC amplitude; modulation frequency = 150 MHz. Panels A, B: amplitude and phase of weight when all three sources are in phase. Panels C, D: amplitude and phase of weight when all source collinear with detector is 180° out of phase with others.

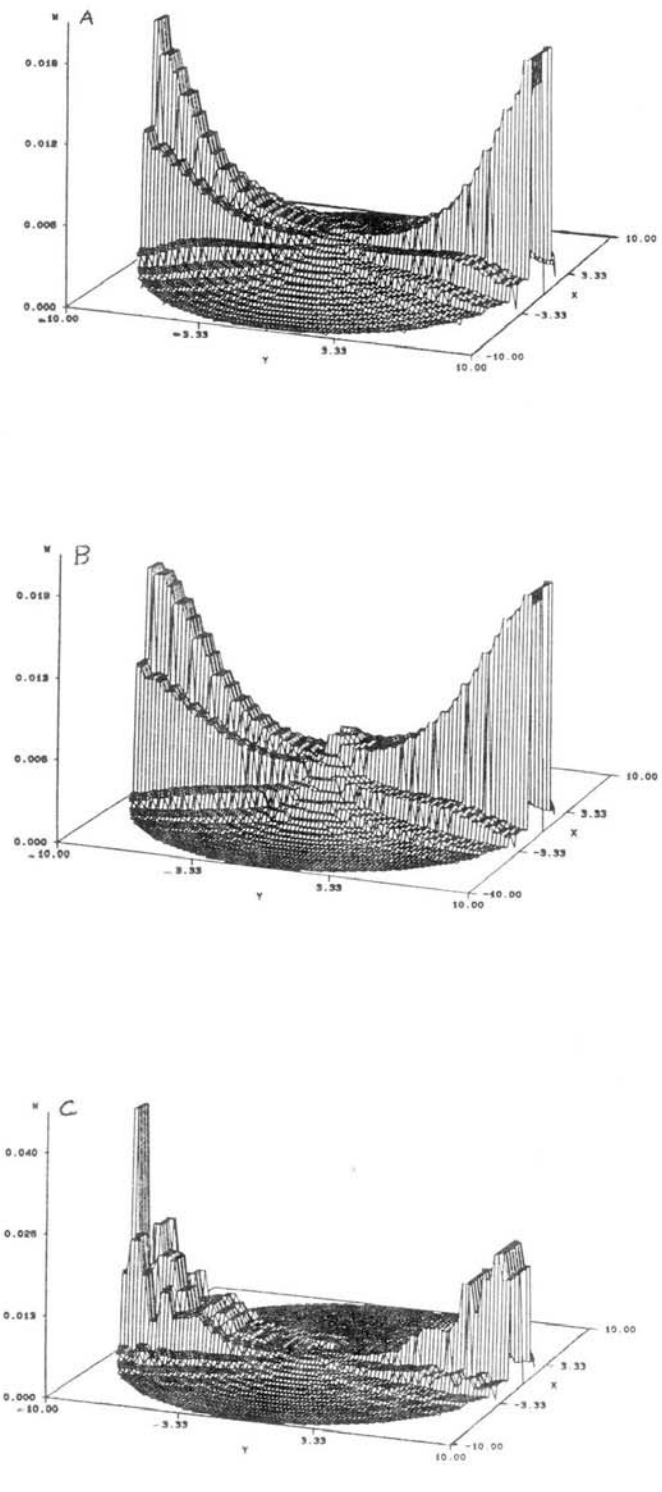

Figure 6 Normalized weight in planar section through cylindrical medium, transmission measurement, for three different illumination strategies. Panel A: steady-state measurement. Panel B: time-domain measurement, detector integration time is first fifty mft following illimination pulse. Panel C: amplitude portion, frequency-domain measurement, modulation frequency is 5.625 GHz.

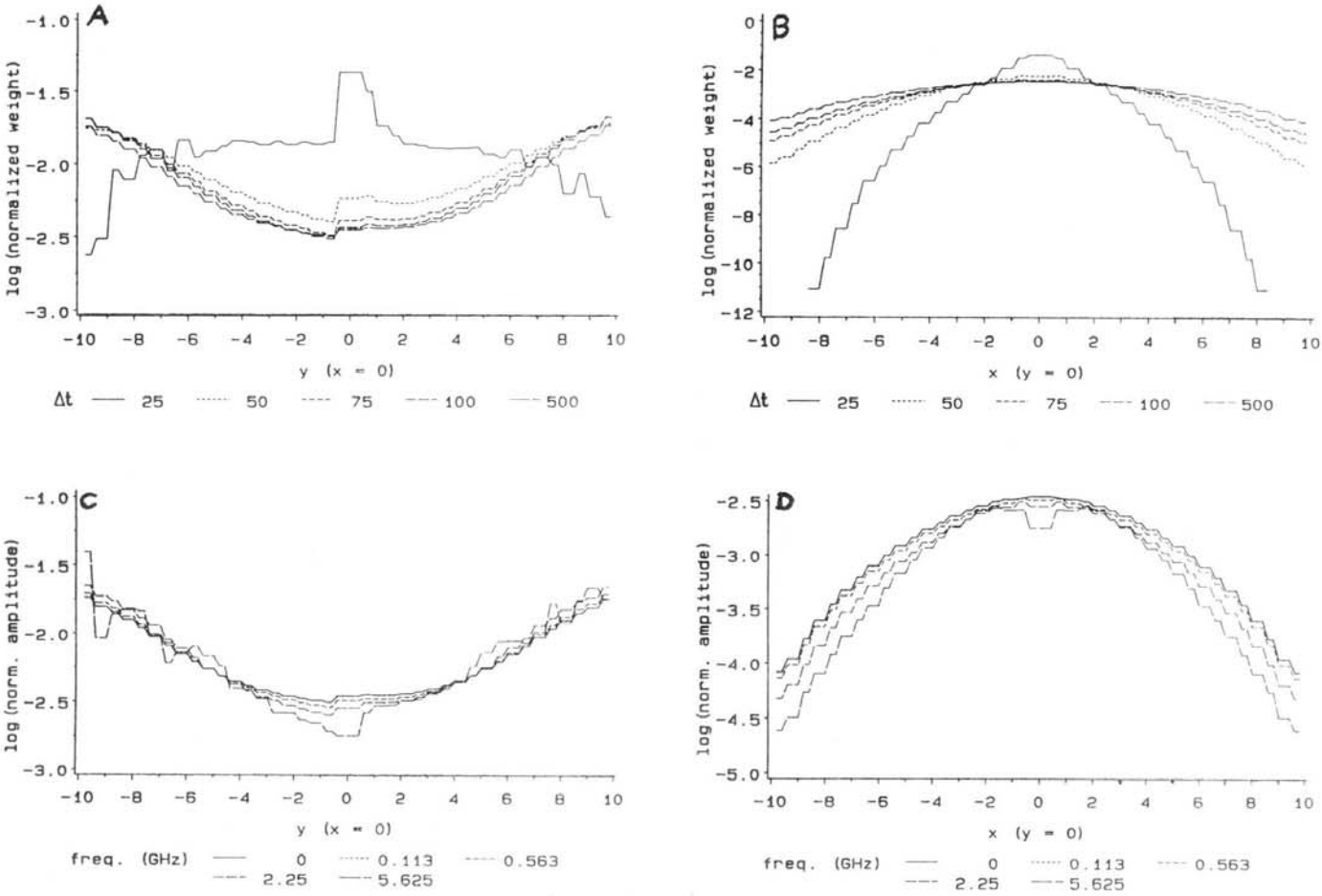

Figure 7 Logarithm of normalized weight *vs.* position along (A and C) or across (B and D) source-detector line, cylindrical medium, transmission measurement. Panels A, B: time domain with increasing integration time at detecor. Panels C, D: frequency domain with increasing source modulation frequency.

studied by members of this group.

Examination of the weight functions for single-source transmission measurements, as well as for other cases in which the source-detector angle was less than 180°, allows us to infer the order in which measurements involving the different illumination and detection schemes could be made and analyzed for optimal spatial resolution. The important features of the results are:

As indicated in Fig. 7A, the weight associated with the earliest arriving nonballistic light is greatest in the center of the cylinder. As the integration time is reduced, the weight declines more rapidly elsewhere along the source-detector line, and more rapidly still in voxels off this line. All photons detected in this time window were necessarily scattered at least once in the interior; the shape of the spatial distribution of weight implies most of these took place near the axis. Photons that scattered in other voxels are much more likely to exit the cylinder at other locations and/or at later times.

In contrast, the amplitude of the frequency-domain weight near the cylinder axis is always relatively smaller than the corresponding steady-state weight. The ratio of amplitude in a voxel at one end of the source-detector line to that at the axis increases with increasing modulation frequency. Consequently, determination of properties in the central region could be made by a process of elimination, using high modulation frequencies to preferentially probe, and fix, the properties of regions near the surface, thereby reducing the number of unknown quantities to be determined from measurements made at low modulation frequencies or at steady-state.

The shifts that take place in the spatial distribution of weight as the integration time is reduced in the time domain, and as the modulation frequency increases in the frequency domain, are

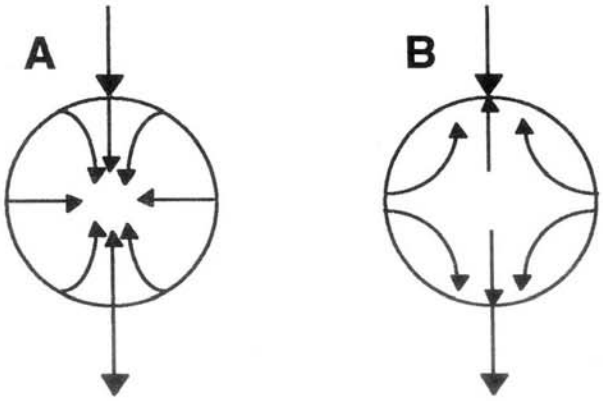

Figure 8 Changes in the spatial distribution of weight, in the case of a transmission measurement and cylindrical medium, due to reducing the detector integration time in the time domain (Panel A) and increasing the modulation frequency in the frequency domain (Panel B).

shown schematically in Figure 8. The arrows in these sketches indicate the directions of migration of the high-weight regions.

As it is unlikely that the optical properties in regions near the axis can be accurately assessed until those in more superficial regions have been determined, the above considerations would suggest that data from a combination of illumination schemes could be analyzed by a layer-stripping algorithm. One approach might be to vary the frequency of modulation to permit optimal analysis of near-surface regions. Improved evaluation of the central region of the medium could then be accomplished by including data from time-resolved measurements.

References

[1] B. Chance, A. Katzir, eds, *Proc. Time-Resolved Spectroscopy and Imaging of Tissues*, SPIE Proceedings Series, vol. 1431, 1991.

[2] B. Chance, R. R. Alfano, A. Katzir, eds., *Proc. Photon Migration and Imaging in Random Media and Tissues*, SPIE Proceedings Series, vol. 1888, 1993.

[3] G. Müller, *et al.*, eds., *Medical Optical Tomography: Functional Imaging and Monitoring*, SPIE Institutes, vol. IS11, 1993.

[4] M. R. Hee, J. A. Izatt, J. M. Jacobson, J. G. Fujimoto, E. A. Swanson, "Femtosecond transillumination optical coherence tomography," *Optics Letters*, vol. 18, pp. 950-2, 1993.

[5] H.L. Graber, J. Chang, R. Aronson, R.L. Barbour, "A perturbation model for imaging in dense scattering media: derivation and evaluation of imaging operators," *Medical Optical Tomography: Functional Imaging and Monitoring*, SPIE Institutes, vol. IS11, pp. 121-43, 1993.

[6] R. L. Barbour, H. L. Graber, Y. Wang, J. Chang, R. Aronson, "A perturbation approach for optical diffusion tomography using continuous-wave and time-resolved data," *Medical Optical Tomography: Functional Imaging and Monitoring*, SPIE Institutes, vol. IS11, pp. 87-120, 1993.

[7] W. Zhu, Y. Wang, H. L. Graber, R. L. Barbour, J. Chang, "A regularized progressive expansion algorithm for recovery of scattering media from time-resolved data," accompanying report in this volume.

Acknowledgment

This work was supported in part by the National Institutes of Health under grant #RO1-CA59955 and by the New York State Science and Technology Foundation.